Supporting Information

Designing Anion-Derived Solid Electrolyte Interphase in Siloxane-Based Electrolyte for Lithium Metal Batteries

Jianyang Wu, [a] *Tianyi Zhou,* [b,c] *Bing Zhong,* [c] *Qian Wang,*,*[d] *Wen Liu,*,*[e] *and Henghui Zhou*,* [a,f]

[a] College of Chemistry and Molecular Engineering, Peking University, 100871 Beijing, China

[b] CAS Key Laboratory of Standardization and Measurement for Nanotechnology, CAS Center for Excellence in Nanoscience, National Center for Nanoscience and Technology, Beijing 100190, China

[c] University of Chinese Academy of Sciences, Beijing 100049, China

[d] Institute of Energy Innovation, College of Materials Science and Engineering, Taiyuan University of Technology, Taiyuan 030024, China

[e] State Key Laboratory of Chemical Resource Engineering, College of Chemistry, Beijing University of Chemical Technology, 100092 Beijing, China

[f] Beijing Engineering Research Center of Power Lithium-ion Battery Beijing 102202, China

Corresponding Author

* E-mail: qianwang19930825@163.com (Q. Wang)

* E-mail: wenliu@mail.buct.edu.cn (W. Liu).

* E-mail: hhzhou@pku.edu.cn (H. Zhou).

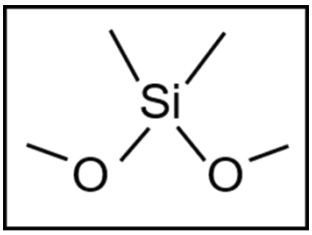

Figure S1. The molecular structure of dimethyl dimethoxy silicane (DMSi).

Electrolytes	Conductivity(mS/cm) at 25 ℃
0.8 M LiFSI+0.2 M LiTFSI+0.05 M $LiNO_3$-DMSi	0.98
0.5 M LiFSI+0.5 M LiTFSI+0.05 M $LiNO_3$-DMSi	0.59
0.2 M LiFSI+0.8 M LiTFSI+0.05 M $LiNO_3$-DMSi	0.015

Table S1. Conductivity data of different electrolytes.

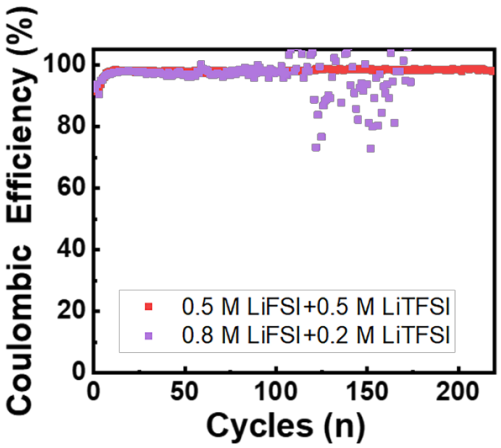

Figure S2. The cycling performance of Li||Cu half cells using different electrolytes at 2 mA cm^{-2}/2 mAh cm^{-2}

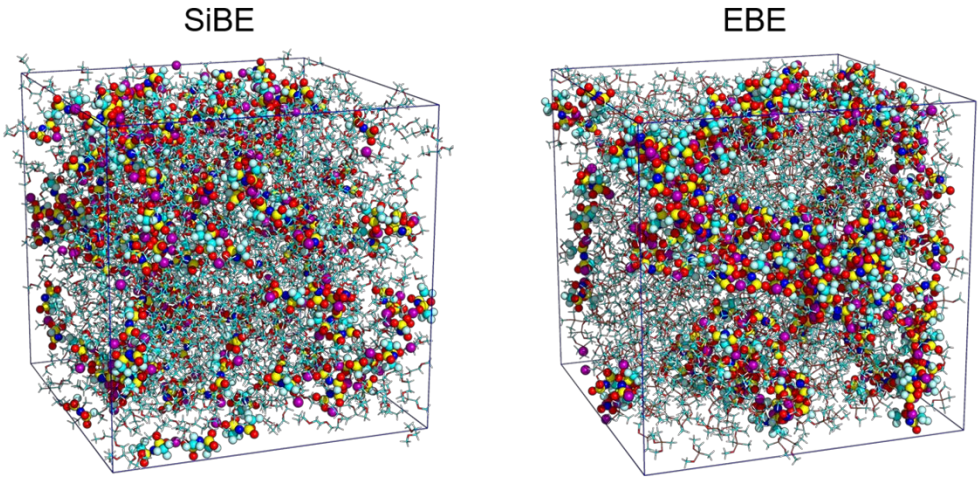

Figure S3. Snapshots of the (a) SiBE and the (b) EBE electrolytes obtained by MD simulations.

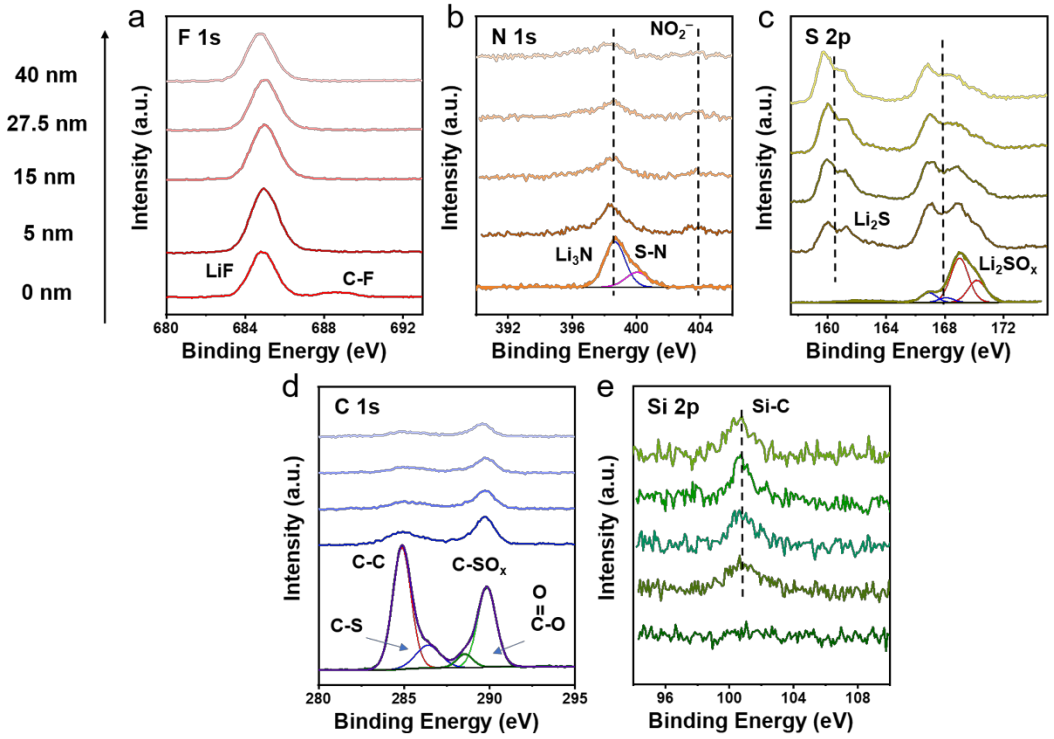

Figure S4. XPS characterization of SEI layers. (a) F 1s, (b) N 1s, (c) S 2p, (d) C 1s and (e) Si 2p spectra at different depths of the Li SEI layers in SiBE.

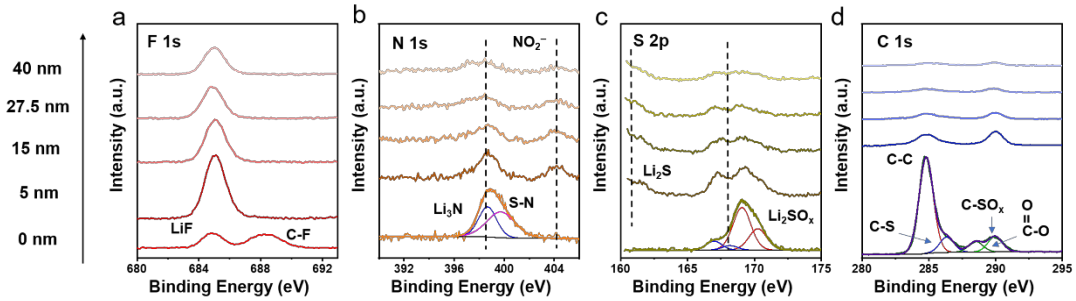

Figure S5. XPS characterization of SEI layers. (a) F 1s, (b) N 1s, (c) S 2p and (d) C 1s spectra at different depths of the Li SEI layers in EBE.

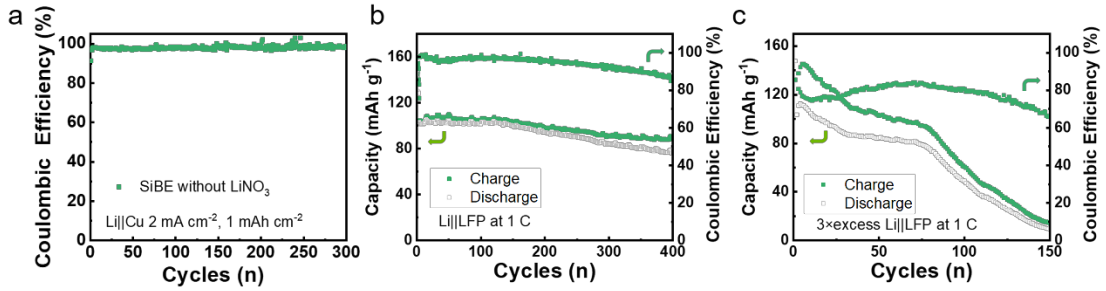

Figure S6. Cycling performance of cells using SiBE without $LiNO_3$. (a) Li||Cu cells at 2 mA cm^{-2}/1 mAh cm^{-2}; (b) Li||LFP cells at 1 C. (c)3×excess Li||LFP cells at 1 C.

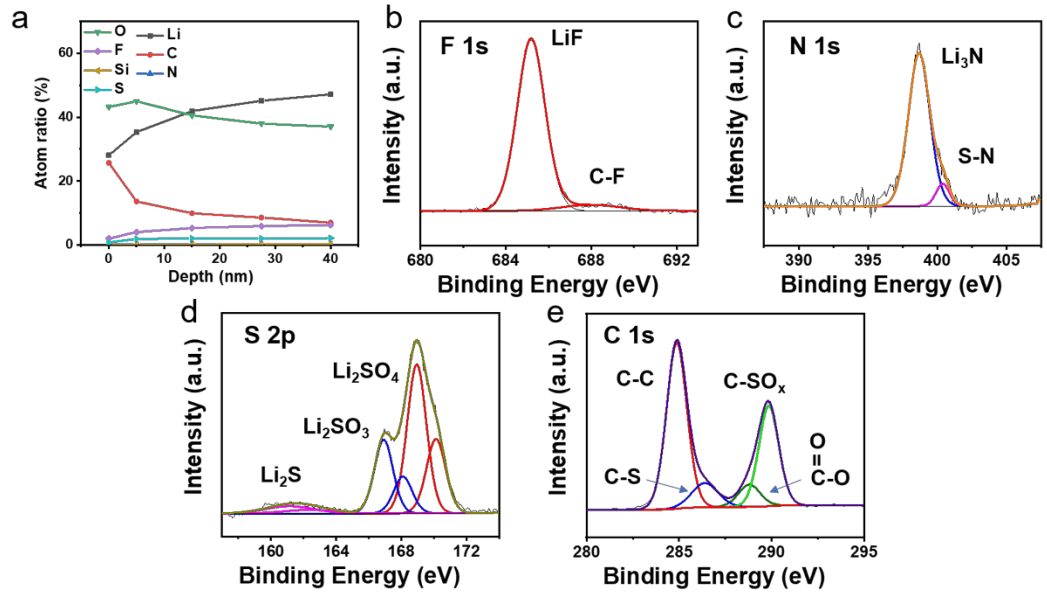

Figure S7. XPS characterization of SEI layers in SiBE without $LiNO_3$. (a) Elemental distributions of the SEI layers with the depth. (b-e) F 1s, N 1s, S 2p, and C 1s spectra of SEI at 0 nm.

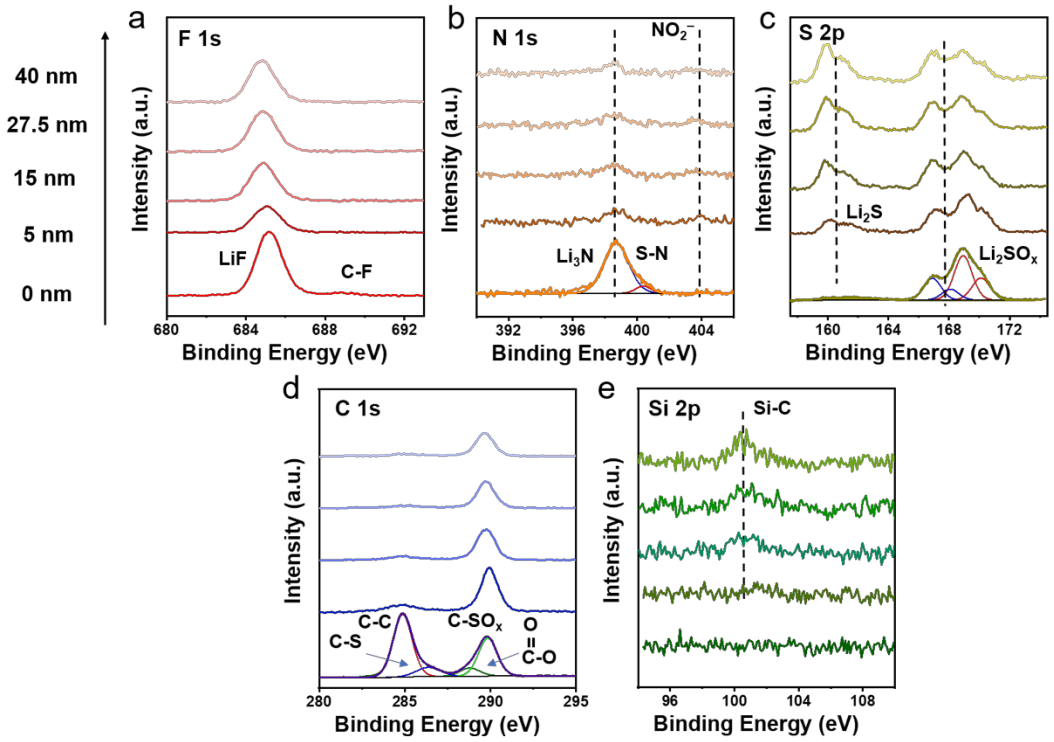

Figure S8. XPS characterization of SEI layers. (a) F 1s, (b) N 1s, (c) S 2p, (d) C 1s and (e) Si 2p spectra at different depths of the Li SEI layers in SiBE without $LiNO_3$.

	C (%)	N (%)	O (%)	F (%)	S (%)	P (%)	Li (%)	Fe (%)
Pristine	47.16	-	9.20	15.98	-	2.14	24.42	0.92
SiBE	33.26	1.70	14.91	14.57	2.58	1.79	29.93	1.02
SiBE no $LiNO_3$	25.56	2.72	30.20	10.06	6.39	0.06	23.93	0.80
EBE	43.16	0.73	18.04	10.02	0.72	1.35	25.03	0.95

Table S2. Elements distributions of CEI layers for LFP cathodes in (a) pristine, (b) SiBE, (c) SiBE without $LiNO_3$, and (d) EBE.

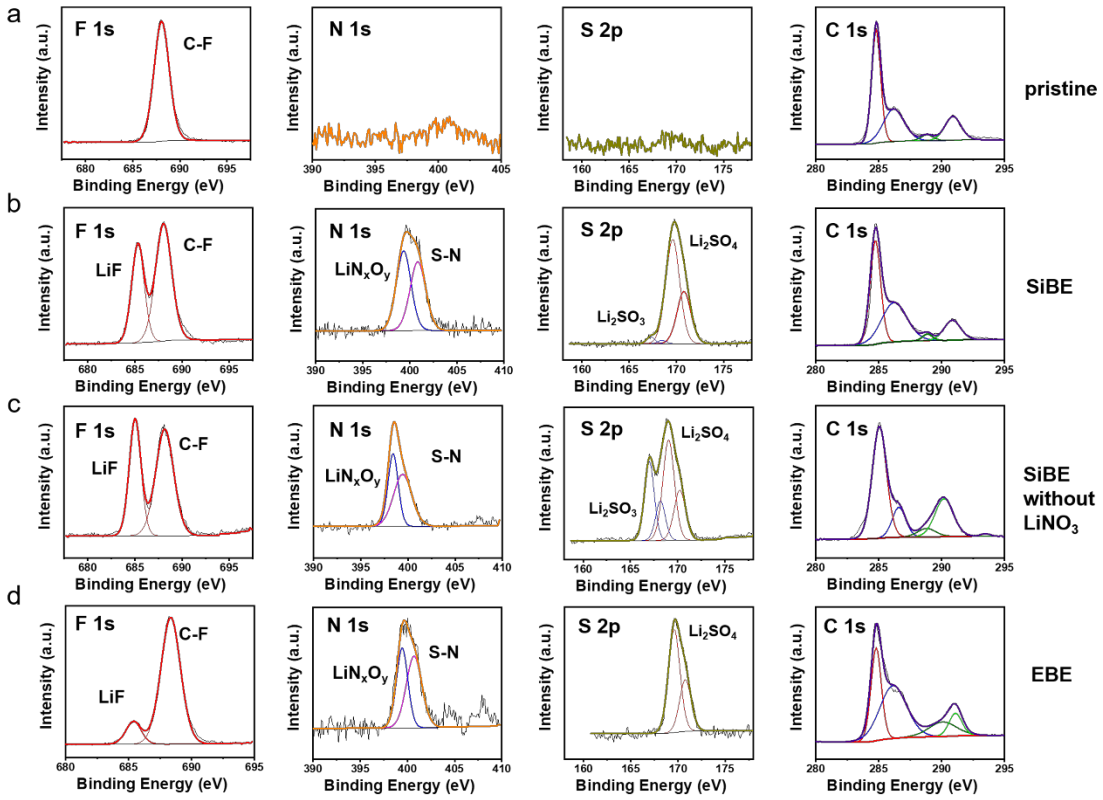

Figure S9. XPS characterization of LFP cathodes in (a) pristine, (b) SiBE, (c) SiBE without $LiNO_3$, and (d) EBE.

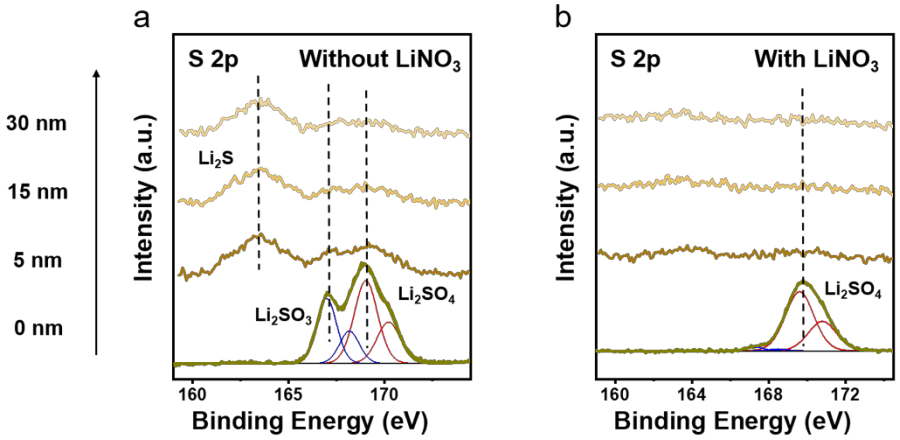

Figure S10. XPS characterization of the CEI layers on LFP cathodes at different depths in (a) SiBE without $LiNO_3$, (b) SiBE with $LiNO_3$.

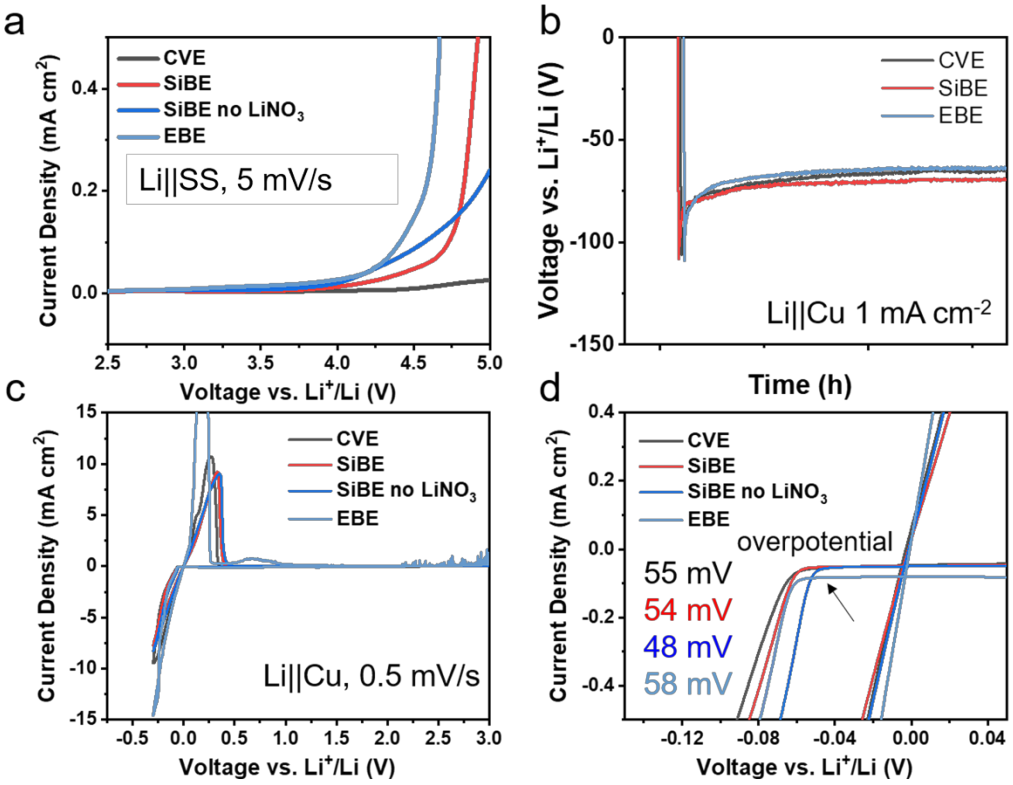

Figure S11. Electrochemical tests for different electrolytes. (a) LSV curves of Li||SS at 5 mV/s within the range of 2.5~5 V; (b) Voltage curves of Li||Cu cells at 1 mA cm^{-2}; (c) CV curves of Li||Cu cells at 0.5 mV/s within the range of -0.3~3 V; (d) the zoom in view of CV curves.

	Nucleation overpotentials (mV)	Growth overpotentials (mV)
SiBE	35.7	72.5
CVE	40.0	66
EBE	45.2	63.9

Table S3. Nucleation overpotentials and growth overpotentials of Li||Cu cells with different electrolytes.

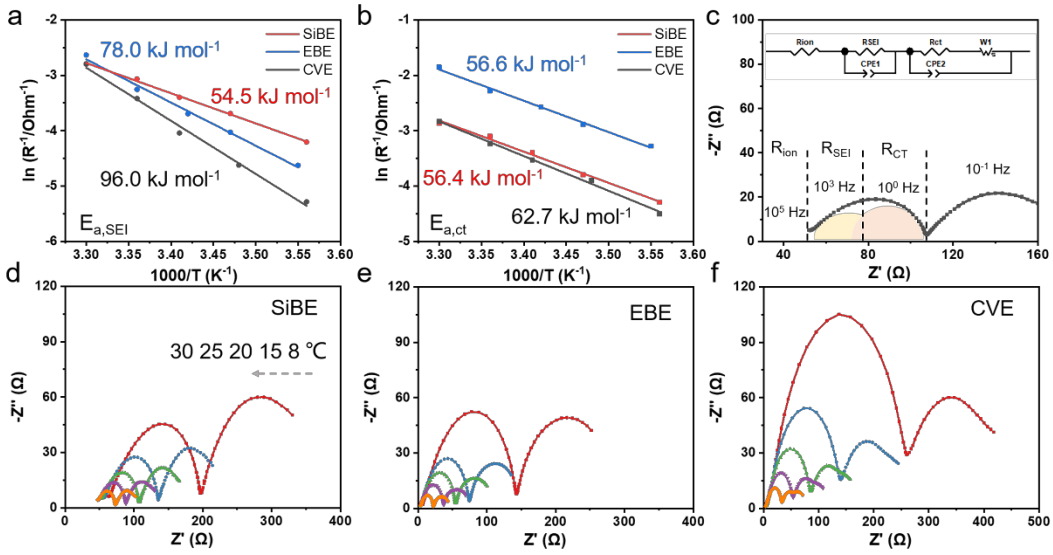

Figure S12. The Arrhenius plots of the activation energy E_a corresponding to (a) Li^+ diffusion through the SEI layers and (b) desolvation. (c) The equivalent circuit model. The resistance-temperature profiles of Li||Li symmetrical cells using (d) SiBE, (e) EBE, and (f) CVE.

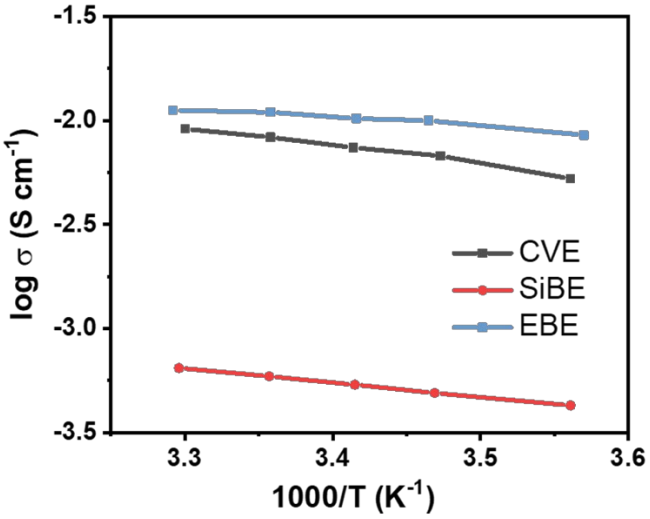

Figure S13. Conductivity-temperature curves of SS||SS with different electrolytes.

Conductivity(mS/cm)	8℃	15℃	20℃	25℃	30℃
CVE	5.21	6.77	7.50	8.34	9.06
SiBE	0.43	0.49	0.53	0.59	0.65
EBE	8.54	9.92	10.12	10.85	11.20

Table S4. Conductivity-temperature data of SS||SS with different electrolytes.

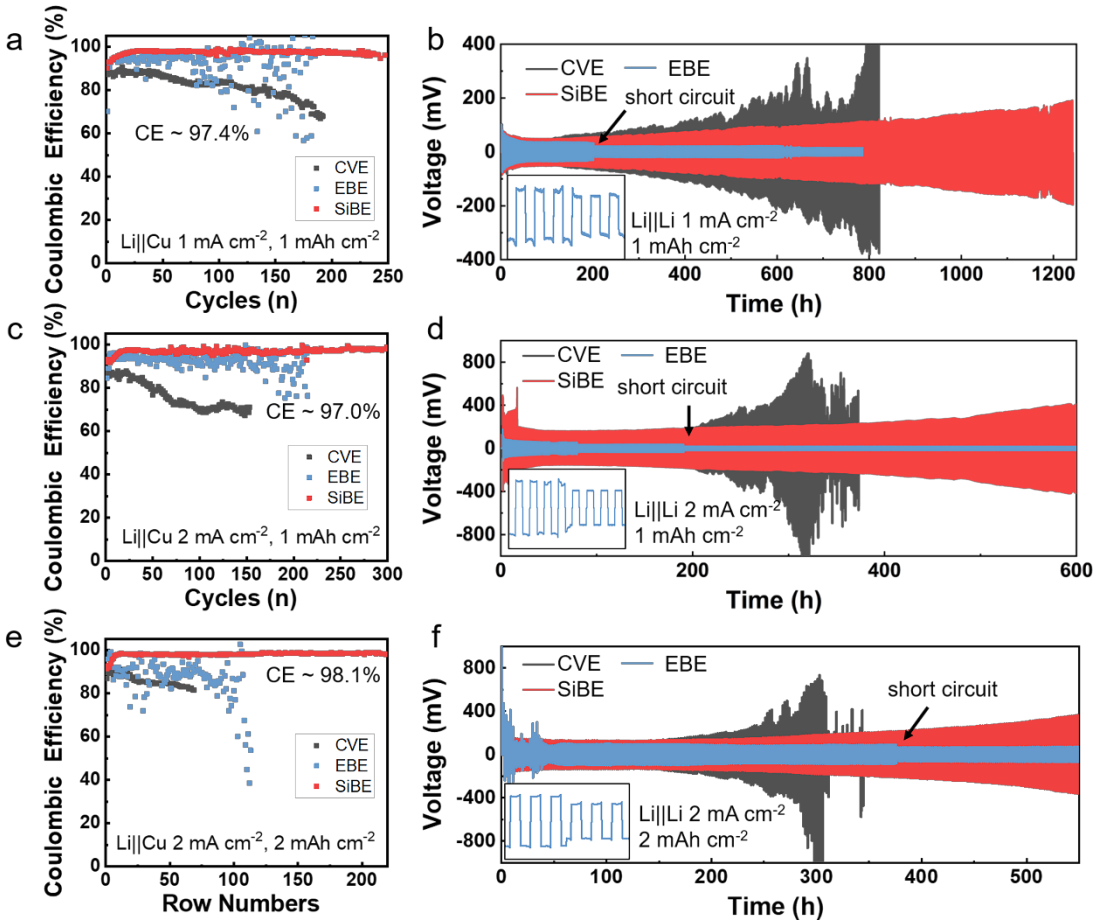

Figure S14. Cycling performance of Li-metal cells using CVE, EBE, and SiBE. (a, c, e) The cycling performance of Li||Cu half cells at 1 mA cm^{-2}/1 mAh cm^{-2}, 2 mA cm^{-2}/1 mAh cm^{-2} and 2 mA cm^{-2}/2 mAh cm^{-2}. (b, d, f) The cycling performance of Li||Li symmetrical cells at 1 mA cm^{-2}/1 mAh cm^{-2}, 2 mA cm^{-2}/1 mAh cm^{-2} and 2 mA cm^{-2}/2 mAh cm^{-2}.

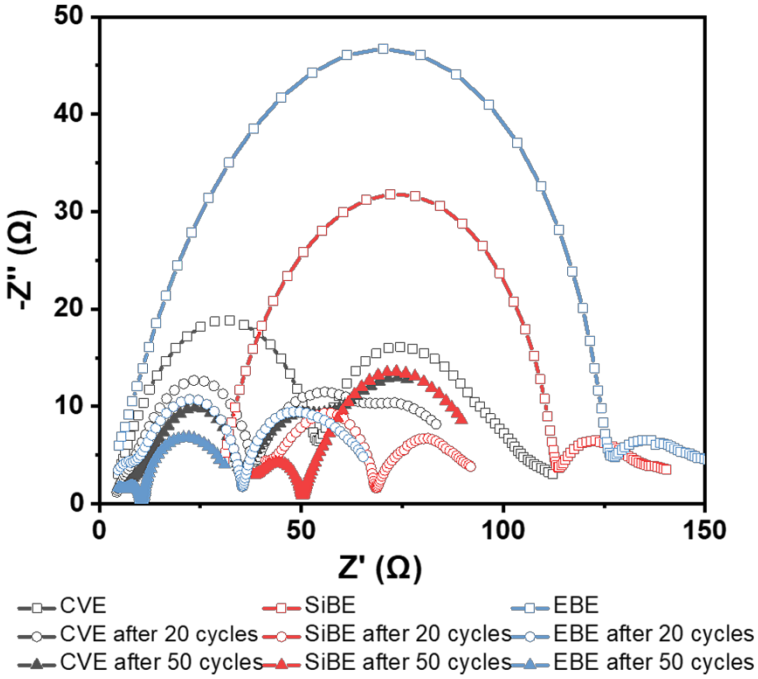

Figure S15. EIS curves of Li||Li cells in different electrolytes after cycles.

Resistance (Ω)	before	20 cycles	50 cycles
CVE-R_Ω	4.7	4.3	6.6
CVE-R_{SEI}	47.2	27.1	25.9
SiBE- R_Ω	31.0	41.2	37.6
SiBE- R_{SEI}	67.2	20.5	10.0
EBE- R_Ω	4.8	4.7	4.7
EBE- R_{SEI}	115.9	27.7	4.4

Table S5. Resistance data of Li||Li cells in different electrolytes after cycles. (R_Ω: ohmic impedance; R_{SEI}: the resistance of Li^+ transport through SEI)

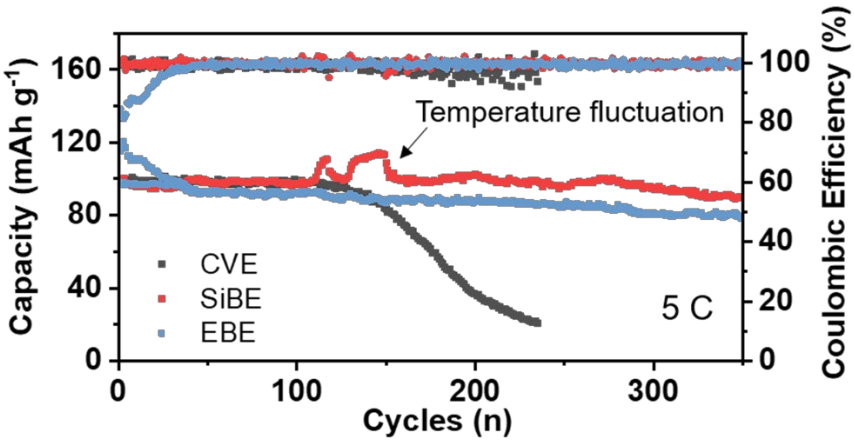

Figure S16. Cycling performance of large-excess Li||LFP using various electrolytes at 5 C.